European Journal of Protistology 93 (2024) 126053

Contents lists available at ScienceDirect

European Journal of Protistology

journal homepage: www.elsevier.com/locate/ejop

Newly identified diversity of Dinomycetaceae (Rhizophydiales, Chytridiomycota), a family of fungal parasites of marine dinoflagellates

Alan Denis Fernández-Valero [a,*], Sergey A. Karpov [b,c,d], Nagore Sampedro [a], Jordina Gordi [a], Natàlia Timoneda [a], Esther Garcés [a], Albert Reñé [a]

[a] Departament de Biologia Marina i Oceanografia, Institut de Ciències del Mar (CSIC), Pg. Marítim de la Barceloneta, 37-49, 08003 Barcelona, Catalonia, Spain
[b] Department of Invertebrate Zoology, Biological Faculty, St Petersburg State University, Universitetskaya nab. 7/9, St Petersburg 199034, Russia
[c] Zoological Institute of Russian Academy of Sciences, Universitetskaya nab. 1, St Petersburg 199034, Russia
[d] North-Western State Medical University named after I.I. Mechnikov, Kirochnaya st. 41, St Petersburg 191015, Russia

ARTICLE INFO

Keywords:
Chytridiomycota
Coastal ecosystems
Dinoflagellate
Fungi
Molecular phylogeny
Ultrastructure
Fungal parasites

ABSTRACT

We identified two new parasite species of Chytridiomycota isolated during blooms of the dinoflagellate *Alexandrium minutum* in the coastal Mediterranean Sea. Light and electron microscopy together with molecular characterization of the nuclear 18S, ITS, and 28S rDNA regions led to their identification as two new species, *Dinomyces gilberthii* and *Paradinomyces evelyniae*, both belonging to the family Dinomycetaceae, order Rhizophydiales. *Dinomyces gilberthii* differs from the previously described *D. arenysensis* by the presence of discharge papillae and the development of a drop-shaped sporangium. *Paradinomyces evelyniae* differs from the previously described *P. triforaminorum* by the prominent lipid globule present in early sporangia and by the pointed end producing a rhizoid. The two chytrids differed in their geographical distribution. *Dinomyces gilberthii* was detected in several Mediterranean habitats, including harbours and beaches, and was particularly prevalent during summer dinoflagellate blooms. Its widespread occurrence in coastal ecosystems suggested a high level of adaptability to this environment. *Paradinomyces evelyniae* had a more restricted distribution in the coastal-marine environment, occurring in harbour sediments and only occasionally in the water column during winter and early spring. *Paradinomyces evelyniae* has previously been detected in the Baltic Sea, suggesting that its distribution encompasses contrasting coastal environments, although its presence is rare.

1. Introduction

Recent environmental sequencing studies of marine protist populations have led to a growing interest in fungi present in marine habitats and their ecological characteristics (Debeljak and Baltar, 2023; Hassett et al., 2019; Pernice et al., 2015; Richards et al., 2015; Tisthammer et al., 2016). The basal fungal clade of Chytridiomycota includes saprotrophs and parasites that infect diatoms (Duan et al., 2018), dinoflagellates (Fernández-Valero et al., 2022; Lepelletier et al., 2014; Reñé et al., 2022), and other marine microorganisms (Gerphagnon et al., 2013; Xue et al., 2018). Infections lead to the death of host cells and can cause the host population to decline (Van den Wyngaert et al., 2022), but parasite and host populations can also coexist (Fernández-Valero et al., 2023). Fungal-host interactions thus have the potential to shape the structure and diversity of marine microbial communities.

Parasitic Chytridiomycota, or chytrids, are a group of zoosporic fungi with a characteristic life cycle. Free-living zoospores attach to the host surface and encyst. After germination, they penetrate the host, often forming rhizoids to absorb nutrients. Cyst growth results in the formation of a sporangium, which contains several nuclei. During sporangium maturation, its multinuclear content differentiates into individual cells, which develop a posterior flagellum and become zoospores. The latter are released through the sporangial wall and infect new host cells (Medina and Buchler, 2020; Trinci et al., 1994). The dependence on a host to complete the life cycle of chytrids defines them as parasitoid fungi, i.e., parasites that consume and eventually kill the host in order to grow and reproduce (Eggleton and Gaston, 1990).

Chytrids have a greater presence in the marine environment than initially believed, which has motivated studies aimed at understanding their ecological role. However, while chytrids have been detected in a large number of environmental sequencing studies. The species identity of those sequences is largely unknown (Grossart et al., 2016), and also

* Corresponding author.
E-mail address: alanfdez.valero@gmail.com (A.D. Fernández-Valero).

https://doi.org/10.1016/j.ejop.2024.126053
Received 12 October 2023; Received in revised form 22 January 2024; Accepted 23 January 2024
Available online 26 January 2024

their ecological function. Identification of these organisms relies on cell isolation and culture efforts, together with microscopic observations. The integration of molecular techniques along with the morphological and ultrastructural characterization allows a correct taxonomic assignment of fungal zoosporic parasites and insights into their specific ecological functions. Indeed, characterizing the diversity of zoosporic fungi in marine environments has been the focus of several studies, covering localities ranging from the Baltic Sea, where *Ericiomyces syringoforeus* Karpov & Reñé (Karpov et al., 2021) and *Paradinomyces triforaminorum* Reñé & Karpov (Reñé et al., 2022) were identified, through the Hebrides Sea, where chytrid strains infecting diatoms have been described (Garvetto et al., 2019), to the Mediterranean Sea, where Fernández-Valero et al. (2022, 2023) examined a broad spectrum of habitats, including seawater, sediment, and epiphytic niches.

Nonetheless, Chytridiomycota are often overlooked in ecological studies, and their role in the marine ecosystem food web, and consequently in nutrient cycling remains poorly understood. In this study, we describe a new diversity in the family Dinomycetaceae Karpov & Guillou (Chytridiomycota), based on the identification of two new species of Chytridiomycota isolated from marine water samples of the coastal Mediterranean Sea. Both parasitize the dinoflagellate *Alexandrium minutum* Halim. These findings have implications for the dynamics of dinoflagellate populations, the main hosts of the new species, in addition to shedding light on chytrid interactions with other organisms in aquatic ecosystems.

2. Materials and methods

2.1. Sampling, isolation and cultivation of chytrids

On March 10th and April 1st 2021, samples were obtained from two harbours along the Catalan coast (NW Mediterranean Sea), Arenys de Mar (41°34′45.5″ N, 2°33′19.8″ E) and Vilanova i la Geltrú (41°12′54.9″ N, 1°43′57.9″ E) (Fernández-Valero et al., 2022), during blooms of the dinoflagellate *A. minutum* (Table 1). Sampling was performed when dinoflagellate abundance in the water column exceeded 10^5 cells L^{-1}. At each location, integrated water column sampling using a tube connected to an electric pump allowed the collection of a 5-L composite sample from a depth range of 2.5–4.0 m, extending from the water surface to the bottom layer. An additional 5-L sample was collected exclusively from the bottom layer. The temperature and salinity of the water samples were measured in situ with a conductivity meter (WTW model Cond 3301), and all laboratory measurements were conducted with the same equipment. Surface sediments were obtained using a sediment corer attached to a pole, with ~ 30 g of sediment collected in a 50-mL Falcon tube using a scoop.

In the laboratory, the seawater samples were filtered through an 80-μm mesh to remove metazoans and large particles. Subsequently, 1 L of each seawater sample was filtered through a 10-μm mesh to retain dinoflagellate cells as well as potential dinoflagellate infections. The 10- to 80-μm fractions were concentrated to 10-mL and incubated in 6-well plates. For sediment samples, portions were placed in double-bottom tubes separated by an 8-μm mesh, with *A. minutum* added on top to promote the vertical swimming of zoospores through the mesh to separate the parasite from the sediment. Incubations were performed in culture chambers at a constant temperature of 20 ± 1 °C with a 12:12 h light:dark photoperiod, with illumination of ~ 40 μmol photons m^{-2} s^{-1} provided by a LED fluorescent tube. The presence of chytrid infections in the incubations was monitored for up to two weeks. Infected dinoflagellate cells were manually isolated to establish clonal chytrid cultures.

Chytrid cultures were maintained in 24-well plates by transferring a 1-mL aliquot of mature sporangia to a new well containing 1 mL of an exponentially growing, uninfected host stock culture every three or four days. Host cultures were maintained under non-axenic conditions in L1 medium with a salinity of 36. Chytrid and dinoflagellate host cultures were maintained under the conditions described above. The dinoflagellate host strains used in this study were obtained from the culture collection of the Institut de Ciències del Mar (ICM-CSIC). *Alexandrium minutum* strain ICMB292 served as a host in the maintenance of newly isolated strain ICMB1106, but the latter also survived with *Ostreopsis* sp. strain ICMB293 as a host. *Ostreopsis* sp. (ICMB293) mixed in equal proportions with *A. minutum* (ICMB292) was used to maintain the newly isolated strain ICMB1107. *Ostreopsis* sp. was chosen because the time required for its consumption by the parasite was longer than that of other dinoflagellates, due to its larger biovolume, thus prolonging the maintenance period of the cultures in the lab.

2.2. Light microscopy

The life cycle of strains ICMB1106 and ICMB1107 was investigated by light microscopy. Regular observations of newly produced infections were conducted to identify the different life-cycle stages and sporangium development. A drop of each chytrid culture was placed on a glass slide and observed with a Nikon Eclipse Ts2R-FL inverted microscope. Photographs were taken with a Nikon DS-10 digital camera, using a PLAN APO 100X magnification objective and differential interference contrast. The NIS Elements v5.3 software was used to capture the images. Time-lapse 40 × photographs from an aliquot of each chytrid strain placed on glass-bottom plates were taken every 10 min for four days using a Zeiss Axio Observer Z1 microscope, an Axiocam 503 mono camera, and the Zen pro 2012 software.

Table 1
Origin and characterization of the studied chytrid strains.

Taxonomic identification	*Dinomyces gilberthii* sp. nov.	*Paradinomyces evelyniae* sp. nov.
Culture code	ICMB1106	ICMB1107
Isolation date	01 April 2021	10 March 2021
Location	Vilanova i la Geltrú	Arenys de Mar
Sampling type	Bottom layer	Integrated water column
Host species in field	*Alexandrium minutum*	
Host abundance (cells L^{-1})	1.1×10^5	9.5×10^4
Salinity	35.4	24.4
Temperature (°C)	15.1	16.3
Host in culture	*A. minutum*	*A. minutum, Ostreopsis* sp.
Culture code of the host	ICMB292	ICMB292; ICMB293
18S rDNA gene	ON081639; ON081640	ON081641; ON081642
Length (base pairs; bp)	1325; 1337	964; 1117
ITS rDNA gene	OQ865234; OQ865235	OQ865236
Length (bp)	643; 607	526
28S rDNA gene	OQ865232; OQ865233	OQ865231
Length (bp)	900; 892	904

2.3. Scanning electron microscopy (SEM)

The structure of the sporangia was examined by SEM. Five mL of ICMB1106 and ICMB1107 cultures containing mature sporangia were fixed in 2% glutaraldehyde for 15 min at room temperature. The ICMB1107 sample was post-fixed with osmium tetroxide with a final concentration of 1% for 15 min at room temperature. The pH was not adjusted. The fixed sporangia were then filtered through a Nucleopore polycarbonate filter (Pleasanton, California, USA) with a diameter of 13 mm and a pore size of 3 μm and washed in distilled water. After dehydration in an ethanol series (25, 50, 75, 90, 96, and 3 × 100%, 10 min each), the filters were critical-point-dried using a Bal-Tec CPD030 apparatus (Leica Microsystems, Vienna, Austria), mounted in holders, and sputter-coated with gold on a Quorum Q150R S (Quorum Technologies, Ltd, Laughton, UK). They were then examined with a variable pressure scanning electron microscope working at 5 kV (Hitachi S-3500 N, Hitachi High Technologies Corp., Japan) at the Servei de Microscòpia Electrònica (ICM-CSIC).

2.4. Transmission electron microscopy (TEM)

The ultrastructure of zoospores was analyzed by TEM. Strains ICMB1106 and ICMB1107 were grown in 6-well plates until a large number of free-living zoospores were observed in the cultures. The supernatant from each well was collected in a 50-mL Falcon tube and centrifuged at 3893 rcf for 6 min at room temperature to concentrate the sample to 2 mL. A threshold concentration of 2.5×10^5 zoospores mL^{-1} was established for initiating block preparation for TEM analysis. The 1.5-mL sample was fixed in 2% glutaraldehyde, postfixed with osmium tetroxide, dehydrated with acetone, and embedded in Spurr resin. Ultrathin serial sections (50–70 nm) obtained using a Leica ultramicrotome UC7 (Leica Microsystems) were stained with 2% uranyl acetate for 10 min and lead-staining solution for 5 min before they were observed with a JEOL JEM-1010 transmission electron microscope fitted with a Gatan Orius SC1000 (model 832) digital camera at the TEM-SEM Electron Microscopy Unit, Scientific and Technological Centers of the University of Barcelona (CCiTUB).

2.5. Molecular procedures and phylogenetic analyses

Individual mature sporangia were isolated from the cultures using glass micropipettes and the single-cell PCR protocol was implemented as described by Reñé and Hoppenrath (2019) and Reñé et al. (2021). The first PCR was performed using the primers EK82F and 28S-1611R (López-García et al., 2001; Moreira et al., 2007) to amplify the entire ribosomal operon followed by (semi-) nested PCR. The region corresponding to the 18S rDNA was amplified using the specific primers CRYPTO22F and EUK1520R (Lazarus and James, 2015; López-García et al., 2003) as reported by Fernández-Valero et al. (2022). The ITS rDNA region was amplified using ITS1 and ITS4 primers (White et al., 1990), and the 28S rDNA region using primers D1R and D3B (Nunn et al., 1996; Scholin and Anderson, 1994). Both ITS and 28S rDNA were amplified in 25-μL reactions containing 1 μL of the first PCR product as template, 2.5 μL of 10 × buffer, 1.5 mM $MgCl_2$, 0.2 mM of each dNTP, 0.4 μM of forward and reverse primers, and 2 U of Taq DNA polymerase. The PCR program was as follows: initial denaturation at 94 °C for 2 min, 35 cycles including denaturation at 94 °C for 15 s, polymerization at 55 °C for 30 s, and elongation at 72 °C for 60 s, followed by a final elongation at 72 °C for 60 s (Reñé et al., 2021). Sanger sequencing with the aforementioned forward and reverse primers was performed by an external service (Genoscreen, France). The molecular sequences obtained were deposited in GenBank with accession numbers OQ865231–OQ865233 (28S rDNA) and OQ865234–OQ865236 (ITS rDNA).

A concatenated 18S rDNA + ITS + partial 28S rDNA dataset covering the diversity of Rhizophydiales Letcher was constructed following that used by Reñé et al. (2022). It was aligned using MAFFT v7 (Katoh and Standley, 2013) and the resulting alignment was manually trimmed to remove poorly aligned positions. The final alignment comprised 52 sequences and 4113 positions. The best-fit substitution model was determined using jModeltest v2.1 (Darriba et al., 2012), resulting in GTR + I + GAMMA under both the Akaike information criterion and the Bayesian information criterion. A maximum likelihood (ML) phylogenetic tree was constructed with RAxML v8.2.12 (Stamatakis, 2014), inferring the best tree from 1000 different starting trees. Bootstrap statistical support was evaluated using 1000 pseudoreplicates. The ML analyses were run at the Marine Bioinformatics Service (MARBITS) of the Institut de Ciències del Mar (ICM-CSIC). A Bayesian reconstruction was conducted using MrBayes v3.2.1 (Ronquist et al., 2012), based on the GTR + I + GAMMA model, four MCMC chains, and 1,000,000 generations. Convergence of the MCMC analyses was confirmed in that the average standard deviation of split frequencies was below 0.01, the potential scale reduction factor was close to 1, effective sample sizes were > 200, and no trends were observed in the plots of generations versus log probability. The first 10% of trees were then considered as burned-in and the Bayesian posterior probabilities (BPP) were determined for the majority rule consensus tree.

2.6. Exploration of metabarcoding datasets

The presence and global distribution of the two species were explored in public V4 18S rDNA metabarcoding datasets, specifically, metaPR2 v2.0.1 (Vaulot et al., 2022), a compilation of 59 published metabarcoding datasets from different surveys that employed environmental metabarcoding targeting the V4 region of the 18S rRNA gene. The search was performed using the 18S rDNA sequences obtained from cultures of ICMB1106 (ON081639) and ICMB1107 (ON081641). These two sequences were also queried for sequence similarity using NCBI-BLASTN against different metabarcoding datasets available from the Catalan coast. Spatial distributions were assessed using the COPAS BioProject PRJNA630546 (Fernández-Valero et al., 2022; Reñé et al., 2021), and temporal distributions using SMART Bioprojects PRJNA1023727 and PRJNA891539. A detection was considered positive when the query coverage was > 80% and the sequence identity > 99%.

3. Results

Chytrids infecting the dinoflagellate *Alexandrium minutum* were detected in samples from the harbours of Vilanova i la Geltrú and Arenys de Mar (Catalan Coast, NW Mediterranean Sea) obtained during blooms of that species (Table 1). In both cases, samples were collected during spring, when the water temperature was 15–16 °C and host abundance was ~ 10^5 cells L^{-1}. The salinity values differed significantly between the two sites, i.e., 35.4 and 24.4, respectively.

3.1. Phylogeny

Molecular analyses were conducted to ascertain the phylogenetic relationships of the two chytrid strains (Fig. 1). Both were determined to belong to the family Dinomycetaceae (order Rhizophydiales). This cluster (99% bootstrap /1.00 BPP) comprised two sister clades, one including *Dinomyces arenysensis* Karpov & Guillou, strain ICMB1106, and *Dinomyces* sp. P242 - RCC3408, and the other including *Paradinomyces triforaminorum* and strain ICMB1107, with maximum statistical support for both. The 28S rDNA (OQ865232, OQ865233) and ITS (OQ865234, OQ865235) sequences of ICMB1106 showed 100% identity with *Dinomyces* sp. P242 - RCC3408 (KJ027549 and KJ027550) sequences, respectively (Supplementary Table S1). The 18S rDNA sequence of *Dinomyces* sp. P242 - RCC3408 was not available. The sequence identity between ICMB1106 and *D. arenysensis* was 98.2% for 18S rDNA, 77.3% for ITS, and 91.6% for 28S rDNA. The sequence

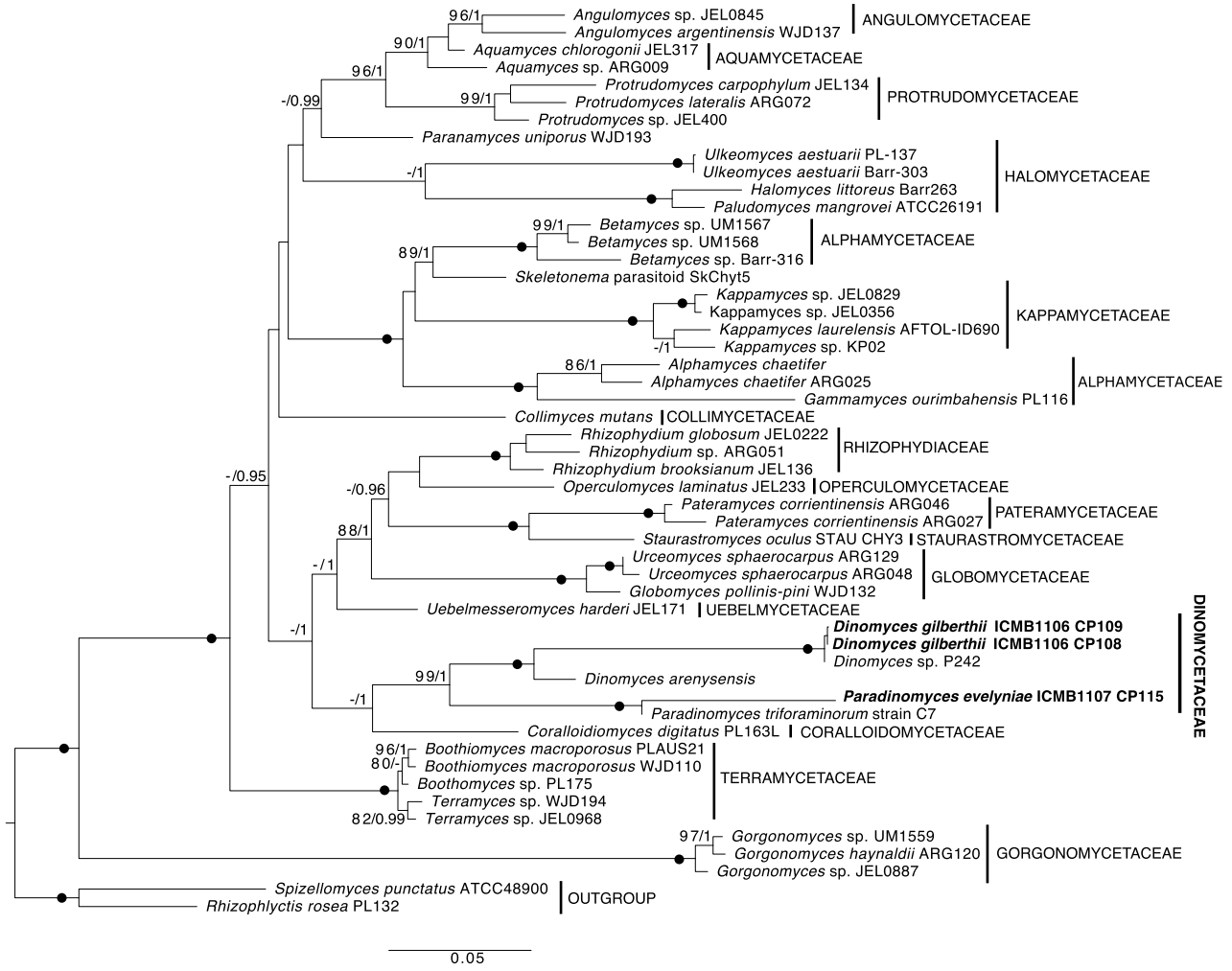

Fig. 1. Phylogenetic tree of Rhizophydiales based on concatenated 18S + ITS + 28S rDNA sequences. Sequences in bold were obtained in this study. *Spizellomyces punctatus* (Spizellomycetales) and *Rhizophlyctis rosea* (Rhizophlyctidales) sequences were used as an outgroup. The numbers above branches indicate the statistical support (ML bootstrap/Bayesian posterior probability); only values > 80% and 0.95, respectively, are shown. Black dots indicate maximum statistical support.

identity of ICMB1107 and *P. triforaminorum* was 98.6%, 83.8%, and 94.5%, respectively. These results justified the designation of strains ICMB1106 and ICMB1107 as representing two new species belonging to the family Dinomycetaceae, namely, *Dinomyces gilberthii* sp. nov. and *Paradinomyces evelyniae* sp. nov., respectively.

3.2. Taxonomy

***Dinomyces gilberthii* sp. nov. Karpov, Fernández-Valero & Reñé**
Order Rhizophydiales Letcher, 2006
Family Dinomycetaceae Karpov & Guillou, 2014
Genus *Dinomyces* Karpov & Guillou, 2014
Index Fungorum: IF 900632.

GenBank accession numbers: ON081639–ON081640 (18S rDNA), OQ865234–OQ865235 (ITS), and OQ865232–OQ865233 (28S rDNA).

Diagnosis: Parasitoid of dinoflagellates with a likely host preference for *Alexandrium minutum*. Drop-shaped epibiotic sporangium 15–25 μm in length on the host *Alexandrium minutum*, with one or two papillae and connected to the host through a rhizoid with an apophysis. Spherical zoospores 2.0–2.6 μm in diameter, with a posterior lipid globule and a flagellum 8–11 μm long. Infects the dinoflagellates *Alexandrium minutum* and *Ostreopsis* sp.

Etymology: The species is named in honour of Gilberth Fernández, the father of the first author of this study.

Type: Fig. 2B.

Type strain: ICMB1106, isolated infecting the dinoflagellate *Alexandrium minutum* in Vilanova i la Geltrú harbour (41°12′54.9″ N, 1°43′57.9″ E), Catalonia (NW Mediterranean Sea), in April 2021.

Hapantotype: Fixed specimen of zoospores and sporangia derived from strain ICMB1106 embedded in a resin block and a stub for electron microscopy, deposited in the Marine Biological Reference Collections (CBMR) at the Institut de Ciències del Mar (ICM-CSIC, Barcelona, Catalonia, Spain) under the accession number ICMCBMR000651 (Guerrero et al., 2023).

Habitat: Marine coastal waters.

Morphological and ultrastructural description of *Dinomyces gilberthii* life-cycle stages

Zoospores of this chytrid species are spherical, with a diameter of 2.0–2.6 μm. They have a posterior flagellum 8–11 μm long and a posterior lipid globule (Fig. 2I). Once attached to the host, the zoospore encysts and a rhizoid with an apophysis develops inside the host cell (Fig. 2B, D, F). The rhizoid branches feed the chytrid and allow the growth of the sporangium (Fig. 2A, B, C, D), which develops one or two papillae (Fig. 2J). Multiple infections are common for this strain, as several zoospores were seen to settle on the host, encyst, and germinate within the dinoflagellate (Fig. 2A, B, G). Furthermore, multiple infections may not occur simultaneously (Fig. 2E, G). The number of infections in a single host cell determines the size of the sporangium and

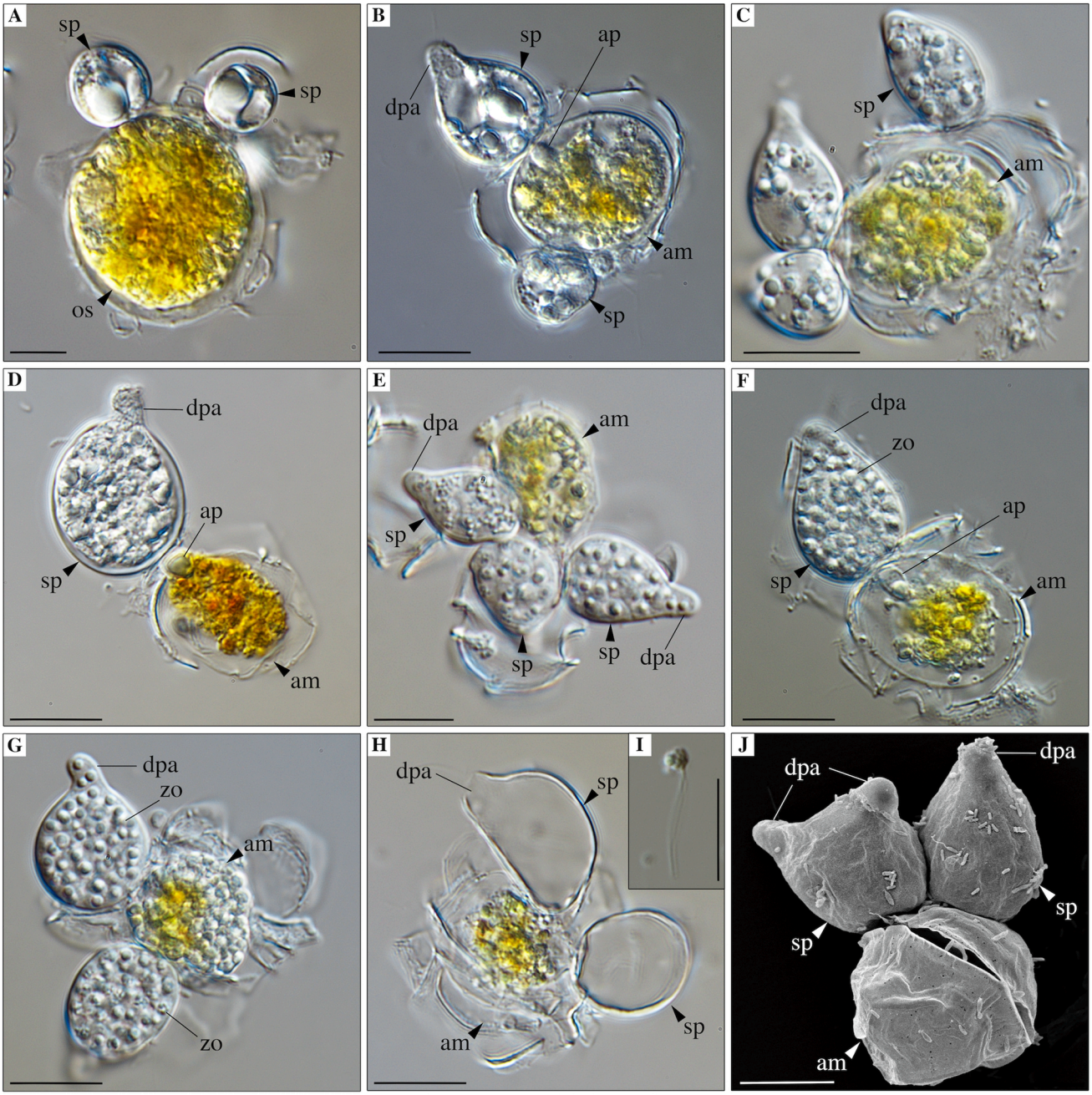

Fig. 2. Life-cycle stages of *Dinomyces gilberthii* sp. nov. in the light microscope (A–I) and in the SEM (J). (**A**) *A. minutum* infected by two young sporangia. (**B, C**) Young sporangium with a developed discharge papilla. (**D**) Sporangium before zoospore formation. (**E**) Sporangia showing the lipid globule compartmentalization during zoospore formation. (**F, G**) Mature sporangium with a discharge papilla. (**H**) Empty sporangium with a discharge papilla. (**I**) Zoospore. (**J**) Two mature sporangia with one and two discharge papillae. Abbreviations: am, *A. minutum*; ap, apophysis; dpa, discharge papilla; os, *Ostreopsis* sp.; sp, sporangium; zo, zoospores. Scale bars: 10 μm.

thus the number of zoospores produced per sporangium. If a host cell is infected by a single zoospore, the final biovolume of the sporangium will be similar to that of the host cell (Fig. 2D, F). However, if there are multiple infections of the same cell, the biovolume of each sporangium will be lower, and so will the number of zoospores produced per sporangium (Fig. 2 E, G). Mature sporangia are drop-shaped, with a length of 15–25 μm when a single infection of an *A. minutum* cell occurs, and typically develop one to two, rarely three, discharge papillae. After reaching its maximum size, sporangia show a gradual compartmentalization of the lipid globule (Fig. 2E, F, G), zoospores begin to individualize, and they are eventually released through the papillae once mature (Fig. 2H). The presence of sporangia with two discharge papillae is common, observed in ~ 29% of sporangia (Fig. 2J), while the development of three discharge papillae is rare (<0.1%, not shown). The complete development of the parasitoid, from the cyst to the mature sporangium and zoospore release, takes ~ 25 h (Supplementary Video S1).

The ultrastructural characters of zoospores are key to the determination of their taxonomic affiliation. The general ultrastructural organization of *Dinomyces gilberthii* zoospores is shown in Fig. 3A–D. The nucleus lies near the center of the cell, slightly shifted towards one side (Fig. 3B–D). The ribosomal core occupies the central part of the zoospores, separating the nucleus from the mitochondrion and the microbody-lipid globule complex. A large lipid globule is present,

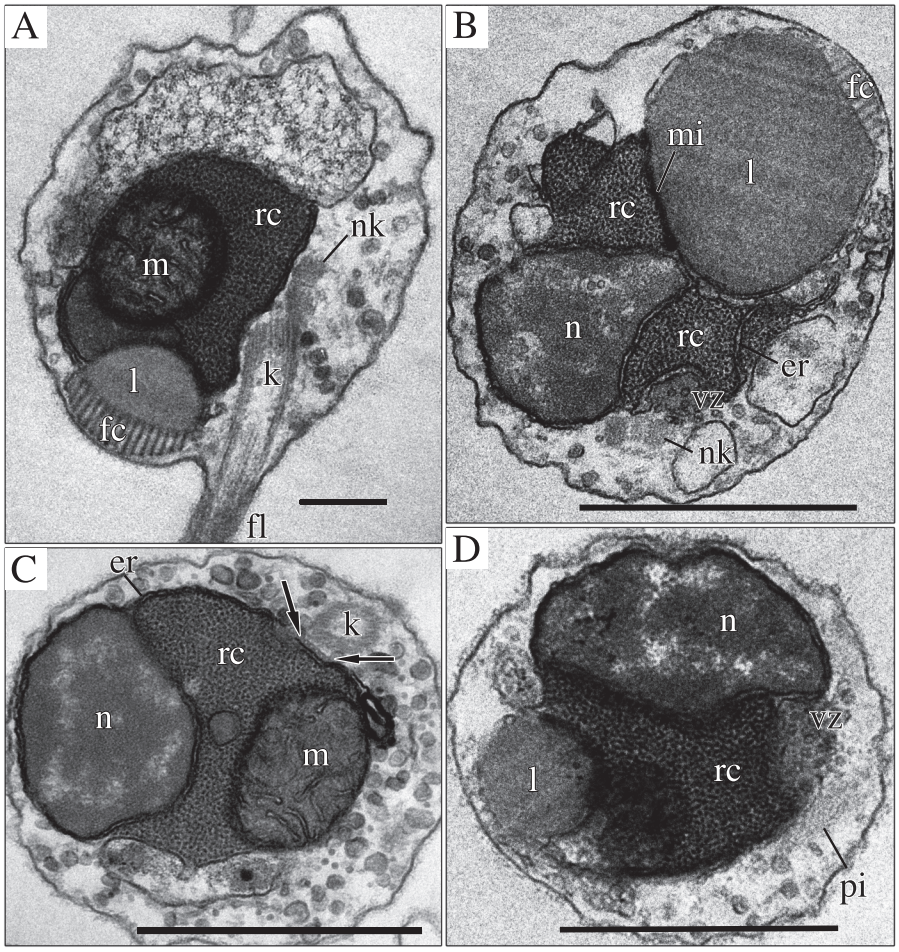

Fig. 3. Ultrastructure of *Dinomyces gilberthii* sp. nov. zoospores. **(A)** Longitudinal section showing the posterior flagellum. **(B–D)** General organelle disposition and cytoskeletal structures in different planes: cross-section of the flagellar kinetosome and five-microtubular root **(C**, arrows), longitudinal section of non-flagellar kinetosome **(B)**, and paracrystalline inclusion **(D)**. Abbreviations: er, endoplasmic reticulum; fc, fenestrated cistern (botrosome); fl, flagellum; k, flagellar kinetosome; l, lipid globule; m, mitochondrion; mi, microbody; n, nucleus; nk, centriole (non flagellar kinetosome); pi, paracrystalline inclusion; rc, ribosomal core; vz, vesiculated zone. Scale bars: 400 nm **(A)** and 1 μm **(B–D)**.

showing a prominent fenestrated cisterna (rumposome) facing the cell surface and covered with a flat microbody (Fig. 3A, B). One mitochondrial profile with flat cristae is attached to the ribosomal core outlined by the endoplasmic reticulum (Fig. 3A–C). Small dense bodies are scattered throughout the dense cytoplasm (Fig. 3A–C) and a vesiculated zone in the cytoplasm is present in the ribosomal core cavity near the kinetid (Fig. 3B, D). At the cell posterior, a paracrystalline inclusion was observed (Fig. 3D). The zoospores also contain a rather prominent vacuole with amorphous contents (Fig. 3A).

The kinetid is composed of a flagellar kinetosome and a short non-flagellar kinetosome (here called a centriole) together forming a 90° angle and connected by a short fibrillary bridge (Fig. 3A). The kinetosome has an anterior root of five microtubules, which is typical for Rhizophydiales (Fig. 3C).

***Paradinomyces evelyniae* sp. nov. Karpov, Fernández-Valero & Reñé**

Order Rhizophydiales Letcher, 2006

Family Dinomycetaceae Karpov & Guillou, 2014

Genus *Paradinomyces* Reñé & Karpov, 2022

Index Fungorum: IF 900676.

GenBank accession numbers: ON081641–ON081642 (18S rDNA), OQ865236 (ITS), and OQ865231 (28S rDNA).

Diagnosis: Parasitoid of dinoflagellates, with a likely host preference for *Alexandrium minutum* and *Ostreopsis* sp. Pear-shaped epibiotic mature sporangium 30–35 μm in length when infecting an *Alexandrium minutum* cell, with a pointed end producing a rhizoid, without papillae. Spherical zoospores 2.1–2.8 μm in diameter, with a single posterior lipid globule and a flagellum 11–13 μm long. Zoospores released from the sporangium through 1–3 discharge pores.

Etymology: The species is named in honour of Evelyn Valero, the mother of the first author of this study.

Hapantotype: Fixed specimen of zoospores and sporangia derived from strain ICMB1107 embedded in a resin block and a stub for electron microscopy, deposited in the Marine Biological Reference Collections (CBMR) at the Institut de Ciències del Mar (ICM-CSIC, Barcelona, Catalonia, Spain) under the accession number ICMCBMR000652 (Guerrero et al., 2023).

Type: Fig. 4D.

Type strain: ICMB1107 isolated infecting the dinoflagellate *Alexandrium minutum* in Arenys de Mar harbour (41°34′45.5″ N, 2°33′19.8″ E), Catalonia (NW Mediterranean Sea), in March 2021.

Habitat: Marine coastal waters.

Morphological and ultrastructural description of *Paradinomyces evelyniae* life-cycle stages

Free-living zoospores of this chytrid species are spherical, with a diameter of 2.1–2.8 μm. They have an 11 to 13 μm-long posterior flagellum and a posterior lipid globule (Fig. 4I). Once the zoospore attaches to a host cell, it encysts. The early trophic phase begins when the cyst

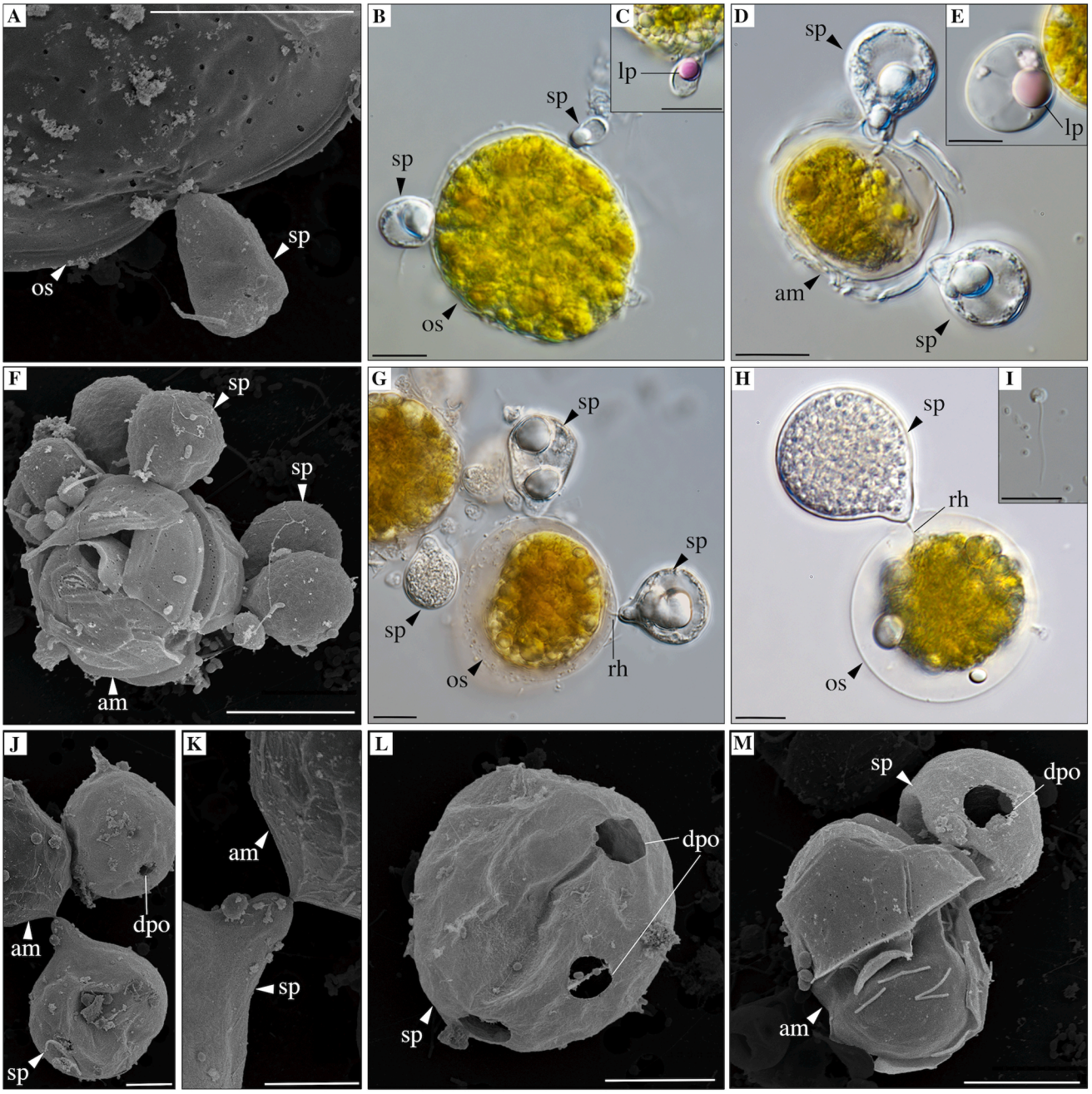

Fig. 4. Life-cycle stages of *Paradinomyces evelyniae* sp. nov. in the light microscope (B, C, D, E, G, H, I) and in the SEM (A, F, J, K, L, M). (**A**) Early sporangium. (**B**) Two young sporangia infecting an *Ostreopsis* sp. cell. (**C**) Nile Red staining of a lipid globule from a young sporangium. (**D**) Development of the infection of two sporangia in a cell of *A. minutum*. (**E**) Growth of the lipid droplet in a Nile Red-stained sporangium. (**F**) Multiple infections in a cell of *A. minutum*. (**G**) Division of the lipid droplet and growth of the sporangium in a cell of *Ostreopsis* sp. (**H**) Mature sporangium containing zoospores. (**I**) Zoospore. (**J, K**) Base of the sporangium connected to a host cell. (**L**) Three open discharge pores of an empty sporangium. (**M**) Empty sporangium with a discharge pore. Abbreviations: am, *A. minutum*; dpo, discharge pore; lp, lipid globule; rh, rhizoid; sp, sporangium; os, *Ostreopsis* sp. Scales bars: 10 μm. (For interpretation of the references to colour in this figure legend, the reader is referred to the web version of this article.)

produces a rhizoid, which penetrates the host cell. Young sporangia are spherical to pear-shaped, with a prominent central lipid globule (Fig. 4B–E). Mature sporangia are pear-shaped, 30–35 μm in length when derived from a single infection of an *A. minutum* cell, and with a pointed end producing the rhizoid (Fig. 4H). Subsequent division of the plasmodium results in the formation of numerous small zoospores (Fig. 4H, I; Supplementary Video S2). The sporangia do not have visible structures related to zoospore discharge. The release occurs through discharge pores instead (Fig. 4J, L, M). The number of infections in the same host cell and the host species biovolume determine the final size of the sporangium (Fig. 4F, H) and the number of zoospores. As infections do not occur synchronously, different stages of infection were observed among sporangia within the same host. The development of the parasitoid, from the cyst to the mature sporangium and release of the zoospores, takes approximately 30 h (Supplementary Video S2).

The general ultrastructural organization of *P. evelyniae* zoospores is shown in Fig. 5. The nucleus lies near the center of the cell, slightly shifted towards one side (Fig. 5A). The ribosomal core occupies the central part of the zoospore, separating the nucleus from the mitochondria and the microbody-lipid globule complex. A large lipid globule

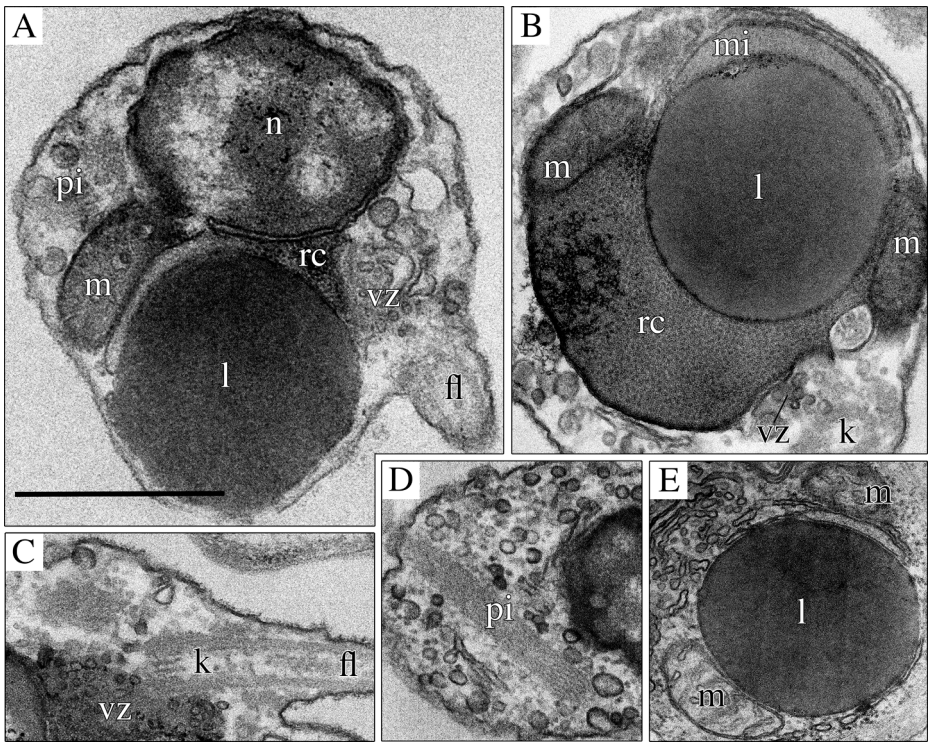

Fig. 5. Ultrastructure of *Paradinomyces evelyniae* sp. nov. zoospores. (**A, B, E**) Nucleus and general organelle disposition. (**C**) Longitudinal section of the kinetosome and flagellum. (**D**) Longitudinal section of paracrystalline inclusion. Abbreviations: fl, flagellum; k, flagellar kinetosome; l, lipid globule; m, mitochondrion; mi, microbody; n, nucleus; pi, paracrystalline inclusion; rc, ribosomal core; vz, vesiculated zone. Scale bar: 500 nm.

is covered with a flat microbody and has no fenestrated cisterna (Fig. 5B). Two mitochondrial profiles with flat cristae are attached to the ribosomal core outlined by the endoplasmic reticulum (Fig. 5A, B, E). Small dense bodies are scattered throughout the dense cytoplasm, with a vesiculated zone seen in the ribosomal core cavity near the kinetid (Fig. 5A, C). A paracrystalline inclusion lies in the cytoplasm near the nucleus (Fig. 5A, D). The kinetid is composed of the flagellar kinetosome (Fig. 5B, C) and a short non-flagellar kinetosome (not shown).

3.3. Geographical and temporal distribution of the novel fungal species

The Chytridiomycota species described in this study were detected in available metabarcoding datasets representing various locations along the Catalan coast (Table 2; Reñé et al., 2021). Examination of the spatial distribution of chytrids along the Catalan coast revealed the presence of *Dinomyces gilberthii* in other harbours (Cambrils, El Masnou and Barcelona) besides Vilanova i la Geltrú (from where it was isolated) during blooms of the dinoflagellate *A. minutum*. It was detected at the beach of Pals during a bloom of the dinoflagellate *Gymnodinium litoralis* Reñé and at the beach at the mouth of the La Muga river, concurrent with a bloom of mixed dinoflagellates dominated by *Prorocentrum micans* Ehrenberg (Reñé et al., 2021) as well. In a study examining the temporal patterns of parasites (unpublished) during coastal dinoflagellate blooms, *D. gilberthii* was detected at El Grau beach during the summer months (late June, July, August) and at L'Estartit beach (late June, July). The dinoflagellate communities in those samples were dominated by *G. litoralis*, but other dinoflagellate species, such as *A. taylori* Balech and *Levanderina fissa* (Levander) Moestrup, Hakanen, Gert Hansen, Daugbjerg & M.Ellegaard, were present as well. In a monthly sampling at Port Olímpic, *D. gilberthii* was detected in the water column during January and December 2022, when the dinoflagellate community was dominated by *A. minutum* and *Prorocentrum triestinum* J.Schiller, respectively. *Dinomyces gilberthii* was also found in sediment samples from January, April, and July 2021. The dominant dinoflagellate in parallel water column samples was *Biecheleria* spp. Seawater temperature and salinity ranges during the detections were 11.8–27.1 °C and 28.6–38.2, respectively (Table 2).

Paradinomyces evelyniae, isolated during an *A. minutum* bloom at Arenys de Mar, was also detected in the water column from El Masnou harbour during *A. minutum* blooms and in sediments from Cambrils harbour. During monthly sampling at Port Olímpic, *P. evelyniae* was detected in seawater during December 2021 and January and December 2022, when the dominant dinoflagellate in the water column was *A. minutum*. The chytrid was also identified in sediment samples obtained in January, February, and May 2022, but was not detected again until December 2022, when *Biecheleria* sp. dominated the water column though other dinoflagellates were present as well. The seawater temperature and salinity ranges of the sampling sites were 11.8–21.9 °C and 36.4–38.0, respectively. *Paradinomyces evelyniae* was also occasionally found in samples from El Grau beach.

Consultation of the metaPR2 database for records of the two species revealed only the presence of *P. evelyniae* in the Baltic Sea. In that case, sampling had been conducted at the Tvärminne zoological station (entrance to the Gulf of Finland, Storfjärden) and in the coastal region of Krogarviken. The species was found in both the surface and the euphotic layer (down to ~ 15 m in depth) at those locations, as well as in the bottom water of Storfjärden, at depths ranging from 15 to 30 m. The temperature and salinity ranges at the sampling sites were 7.3–11.5 °C and 5.4–6.2, respectively (Table 2).

4. Discussion

4.1. Identity and characteristics of the newly described species

The present phylogenetic tree based on 18S, ITS, and 28S rDNA sequences showed two main clades within Dinomycetaceae. One included

Table 2
Origin of amplicon sequence variants (ASVs) detected by metabarcoding and identified as *D. gilberthii* sp. nov. & *P. evelyniae* sp. nov., and characteristics of corresponding samples.

Species	Type	Location	Sampling date	Compartment	Dominant dinoflagellate	Temperature (°C)	Salinity	ASV match and reference
Dinomyces gilberthii	Harbour	Cambrils[1]	15 MAY 2019	seawater, sediment	*Alexandrium minutum*	18.7	36.9	ASV84; Reñé et al. (2021)
		Barcelona[1]	28 MAR 2019	seawater, sediment		15.3	38.2	
		El Masnou[1]	2 MAR 2018	seawater		11.8	37.7	
			7 MAR 2018	seawater, sediment		13.2	38.0	
	Beach	La Muga[1]	5 JUN 2019	seawater	mixed dinoflagellates dominated by *Prorocentrum micans*	26.4	37.4	
		Pals[1]	4 JUL 2019	seawater, sediment	*Gymnodinium litoralis*	21.5	35.7	
	Harbour	Port Olímpic[1]	11 JAN 2022	seawater	*A. minutum*	12.9	36.6	ASV4101; Unpublished results
			11 JAN 2022	sediment	*Biecheleira* spp.	12.9	36.6	
			26 JAN 2022	sediment		12.7	37.0	
			5 APR 2022	sediment	*Biecheleria* sp., *Alexandrium ostenfeldii*	13.2	36.4	
			29 JUL 2022	sediment	*Pyrophacus steinii*, *Biecheleria* sp.	27.1	37.6	
			15 DEC 2022	seawater	*Prorocentrum triestinum*	14.7	36.4	
	Beach	ĹEstartit[1]	21 JUN 2022	seawater	*G. litoralis*	21.7	37.0	
			29 JUN 2022	seawater	*G. litoralis*, *Alexandrium taylori*, *Levanderina fissa*	24.4	37.2	
			08 JUL 2022	seawater	*Heterocapsa* spp.	22.8	37.3	
		El Grau[1]	21 JUN 2022	seawater	*G. litoralis*	22.9	32.9	
			08 JUL 2022	seawater		23.0	35.9	
			18 JUL 2022	sediment	*A. taylori*	26.9	30.3	
			27 JUL 2022	seawater	*G. litoralis*	26.3	28.6	
			19 AUG 2022	seawater	*Heterocapsa* sp.	24.6	37.5	
Paradinomyces evelyniae	Harbour	Cambrils[1]	15 MAY 2019	sediment	*A. minutum*	18.7	36.9	ASV613; Reñé et al. (2021)
		El Masnou[1]	2 MAR 2018	seawater		11.8	37.7	
			7 MAR 2018	seawater, sediment		13.2	38.0	
	Harbour	Port Olímpic[1]	14 DEC 2021	seawater	*A. minutum*	14.3	36.5	ASV5858; Unpublished results
			11 JAN 2022	seawater		12.9	36.6	
			11 JAN 2022	sediment	*Biecheleira* sp.	12.9	36.6	
			26 JAN 2022	sediment	*Biecheleria* sp., *Pyrophacus steinii*	12.7	37.0	
			23 FEB 2022	sediment	*Biecheleria* sp.	14.0	36.9	
			19 MAY 2022	sediment	*Heterocapsa* sp., *Suessiaceae*	21.9	36.8	
			15 DEC 2022	seawater	*Prorocentrum triestinum*	14.7	36.4	
	Beach	Grau[1]	19 AUG 2022	sediment	*Heterocapsa* sp.	24.6	37.5	
	Shallow semi-enclosed bay	Krogarviken[2]	8 OCT 2012	water	*Heterocapsa triquetra*, *Biecheleria baltica*, *Dinophyceae* sp.	11.6	6.1	ASV New1465; Enberg et al. (2018)
	Deep bay	Storfjärden[2]	8 OCT 2012	surface water	*Heterocapsa triquetra*, *Biecheleria baltica*	11.9	6.0	
			8 OCT 2012	bottom water	*Heterocapsa triquetra*, *Biecheleria baltica*	11.9	6.1	
			19 OCT 2012	bottom water	*Biecheleria baltica*	7.3	6.3	
			29 OCT 2012	surface water	*Heterocapsa triquetra*, *Biecheleria baltica*	9.0	5.4	
			29 OCT 2012	bottom water	*Gymnodinium corollarium*	10.5	5.6	

[1] NW Mediterranean Sea, [2] Baltic Sea.

Dinomyces arenysensis and the new species *D. gilberthii*, while the other comprised *Paradinomyces triforaminorum* and the new species *P. evelyniae*. The identity between sequences belonging to the same clade was > 98% for 18S rDNA, >70% for ITS, and > 90% for 28S rDNA, while the identity between sequences belonging to different clades was much lower. As mentioned above, *D. gilberthii* corresponds to the species previously recorded as *Dinomyces* sp. P242 - RCC3408 (Lepelletier et al., 2014). Morphological or ultrastructural information was not provided in that report, and the species was tentatively classified as a *Dinomyces* representative based on the low divergence between its ITS and 28S rDNA sequences and those of *D. arenysensis*. Our results are in agreement with that interpretation.

The morphological, ultrastructural, and molecular results obtained in this study justify the description of the species included in each clade as belonging to the genera *Dinomyces* and *Paradinomyces*. A morphological distinction between them is in that the sporangia of *D. gilberthii* and *D. arenysensis* have an apophysis, whereas those of *P. evelyniae* and *P. triforaminorum* have branched rhizoids. Ultrastructural differences were also observed between the respective zoospores. Zoospores of *D. gilberthii* have fenestrated cisternae and kinetid characteristics similar to those of *D. arenysensis*, whereas the zoospores of *Paradinomyces triforaminorum* and *P. evelyniae* lack fenestrated cisternae. Although the kinetid was not studied in detail, that of *D. gilberthii* has the same anterior five-microtubular root seen in kinetids of other Dinomycetaceae, and an inclined kinetosome orientation was found in both *D. gilberthii* and *P. evelyniae*. Zoospores of the two strains contain a paracrystalline inclusion, as also found in *P. triforaminorum* (Reñé et al., 2022). A paracrystalline inclusion was not detected in zoospores of *D. arenysensis* (Lepelletier et al., 2014), but the reinvestigation of its original TEM images revealed a bundle of microtubules at the zoospore's anterior side, as visible in Fig. 4D of Lepelletier et al. (2014). The paracrystalline inclusion consists of a pool of tubulins that may also assume a microtubular appearance, as observed in zoospores of *P. evelyniae* (Fig. 5). Given that zoospores of all described members of Dinomycetaceae contain a paracrystalline inclusion, it can be regarded as a character of the whole family.

Regarding interspecies differences, the two strains differ genetically and morphologically from the previously described species of *Dinomyces* and *Paradinomyces*. In the case of *Dinomyces*, the sporangia of *D. gilberthii* exhibit a drop-shaped growth derived from the development of discharge papillae for zoospore release. This structure is lacking in *D. arenysensis*, whose sporangia are more spherical. Furthermore, zoospores of these two species differ in their dimensions. In the case of *Paradinomyces*, early sporangium development in *P. evelyniae* is marked by a prominent lipid globule. In addition, the sporangia of *P. triforaminorum* have three openings for zoospore release, whereas *P. evelyniae* has a variable number (1–3) of discharge pores. However, zoospores of the two *Paradinomyces* species are of the same dimensions and have the same general ultrastructure.

4.2. Factors influencing the distribution and behaviour of Dinomyces and Paradinomyces species in marine environments

Both the establishment of chytrid-dinoflagellate interactions and the characterization of host preferences can be challenging when based only on metabarcoding information. However, it is clear that chytrid occurrence is influenced by the presence of preferred protist hosts, as demonstrated in the present study and that of Fernández-Valero et al. (2022). *Dinomyces gilberthii* was detected in various locations along the Catalan coast, both on beaches during summer and in harbour sediments throughout the year. This widespread coastal distribution of *D. gilberthii* highlights its adaptability. The role of this species in the dynamics of coastal dinoflagellate blooms could be similar to that studied in *D. arenysensis*, which varies from host-parasite coexistence (observed in the field and laboratory experiments) to near extinction of the host population (observed in laboratory experiments) (Fernández-Valero et al., 2023).

The persistence of *D. gilberthii* in the water column during spring and summer coincided with high biomass blooms of the dinoflagellates *A. minutum* and *G. litoralis* or mixed communities dominated by these dinoflagellates. However, despite the co-occurrence of *G. litoralis* blooms and *D. gilberthii* indicated by metabarcoding datasets, attempts to induce infections of *G. litoralis* strain ICMB235 in the laboratory were unsuccessful (data not shown). In previous research, the inability of *Dinomyces* sp. P242 - RCC3408 (=*D. gilberthii*) to infect *G. litoralis* (strain ICMB226) was observed in cross-infection experiments (Lepelletier et al., 2014). Co-occurrence in the field but failure infections in the laboratory suggest strain-strain incompatibilities or *D. gilberthii*'s preference for alternative species during *G. litoralis* blooms. The need for further exploration of the chytrid's host range, with early indications of specificity for members of the genera *Alexandrium* Halim, *Scrippsiella* Balech, and *Ostreopsis* J. Schmidt (Lepelletier et al., 2014), is a reminder of the caution required when interpreting the simultaneous presence of two species in a metabarcoding dataset, as it may not represent a definitive relationship between them.

In contrast to *D. gilberthii*, *P. evelyniae*, with a more restricted occurrence in the water column, was mainly detected in harbour sediments, during winter and early spring, despite an exceptional detection in beach sediments in summer. The presence of *A. minutum*, one of the *P. evelyniae*'s dinoflagellate hosts, in the water column may have influenced the occurrence of the chytrid. Its more limited distribution along the Catalan coast, i.e., only during *A. minutum* blooms, compared to that of *D. gilberthii*, suggests a higher host specificity.

The frequent detection of chytrid-dinoflagellate pairs in coastal ecosystems implies greater importance of biotic factors, especially the host presence, than abiotic factors in the parasite development. On the other hand, the detection of chytrids in sediments points to this compartment as a species reservoir, when primary hosts are absent from the water column. Nonetheless, abiotic factors may also influence species distribution. The presence of *D. gilberthii* and *P. evelyniae* in Mediterranean samples and the occurrence of *Paradinomyces* spp. in the Baltic Sea question previous conclusions regarding the abiotic preferences of chytrids with respect to salinity. Notably, *P. triforaminorum* was previously described in low-salinity waters from the Baltic Sea during a bloom of the dinoflagellate *Kryptoperidinium foliaceum* (F.Stein) Lindemann (Reñé et al., 2022), and *P. evelyniae* was detected in Northern Baltic Sea waters (Enberg et al., 2018). Further studies on how salinity modulates the geographical distribution of chytrids could provide deeper insights into their ecological dynamics within diverse aquatic ecosystems, especially for species able to adapt and survive in marine ecosystems, which thus far are assumed to include only a few (Rojas-Jimenez et al., 2019).

Indeed, zoosporic fungi have been described as being less resistant to marine environments than other fungal groups, such as Basidiomycota and Ascomycota (Jones et al., 2022) and they show optimal growth under low salinity conditions (Guo et al., 2023). This may explain why locations, such as the Baltic Sea or sea ice, host a relatively high proportion of chytrids (Hassett et al., 2019). However, the same study also mentions locations of the Mediterranean Sea and Red Sea, both of which are characterized by high salinity and the presence of a high richness of Chytridiomycota. Therefore, whether salinity is a key factor in the chytrid biogeography is still an open debate.

Our study offers perspectives on the spatial and temporal distribution of two newly identified marine chytrids, including their recurrent presence in specific localities. Repetitive occurrences may be mainly influenced by the presence of the species in sediments along the year and host availability in the water column. The description of these species expands our understanding of the biological components that interact directly with dinoflagellate species, revealing added complexity in the dynamics of phytoplankton blooms. In the absence of primary hosts, parasites able to infect secondary hosts or enter dormant states (in the sediments) would have strong survival advantages. Both survival

mechanisms and the persistence of *D. gilberthii* and *P. evelyniae* in the sediment reservoirs remain to be examined in order to elucidate the direct role of these chytrid species in the coastal ecosystems.

Assessing the global presence of Chytridiomycota species in metabarcoding datasets from marine regions is challenging due to limited detections in global molecular datasets. The scarcity of these detections can be attributed to inadequate sampling efforts, particularly in regions where these fungi occur prominently, such as in the benthic and epiphytic compartments (Fernández-Valero et al., 2022). Additionally, limitations may arise from the lack of sampling during conditions favorable for chytrid growth, such as microalgal blooms (Fernández-Valero et al., 2023).

Undetected taxa are not proof of absence because a rare biosphere might not be revealed by metabarcoding due to insufficient sequencing depth. This study underscores the need to employ diverse sampling methods in diverse habitats and to integrate molecular and morphological techniques to gain a thorough understanding of the lesser-studied fungal diversity within marine ecosystems.

CRediT authorship contribution statement

Alan Denis Fernández-Valero: Investigation, Methodology, Writing – original draft, Writing – review & editing. **Sergey A. Karpov:** Writing – original draft, Visualization, Validation, Supervision, Formal analysis. **Nagore Sampedro:** Writing – review & editing, Resources, Methodology. **Jordina Gordi:** Resources, Methodology. **Natàlia Timoneda:** Visualization, Validation, Software, Methodology, Investigation, Formal analysis, Data curation. **Esther Garcés:** Writing – review & editing, Writing – original draft, Investigation, Funding acquisition, Data curation, Conceptualization. **Albert Reñé:** Writing – review & editing, Writing – original draft, Methodology, Investigation.

Declaration of Competing Interest

The authors declare that they have no known competing financial interests or personal relationships that could have appeared to influence the work reported in this paper.

Data availability

Data will be made available on request.

Acknowledgements

This study was funded by the Spanish MICINN Project SMART PID2020-112978GB-I00, with institutional support from the "Severo Ochoa Centre of Excellence" (CEX2019-000928-S). A. D. Fernández-Valero was funded by the MICIU grant "Ayudas para contratos predoctorales para la formación de doctores 2018" (PRE2018-084893). This work was partly supported by the Russian Science Foundation, grant no. 21–74–20089 (light and electron microscopy analysis, manuscript writing). SAK thanks Saint-Petersburg State University for a research grant (project ID Pure 115624290) and ZIN RAS program 122031100260-0. We thank the TEM-SEM Electron Microscopy Unit from Scientific and Technological Centers (CCiTUB), Universitat de Barcelona, and its staff for their support and advice during the TEM studies. We thank Dr. J-M. Rintala (University of Helsinki, Finland) and Dr. M. Majaneva (Norwegian Institute for Nature Research, Norway) for providing metadata from their metabarcoding dataset. We also thank Dr. M. Antó and Dr. I. Ruiz (Institut de Biologia Evolutiva IBE-CSIC) for their time and for providing access to their laboratory equipment.

Data availability statement

Molecular sequences generated in this study are publicly available in GenBank. Phylogenetic alignments analysed in the present study are available from the corresponding author upon request.

Appendix A. Supplementary data

Supplementary data to this article can be found online at https://doi.org/10.1016/j.ejop.2024.126053.

References

Darriba, D., Taboada, G.L., Doallo, R., Posada, D., 2012. jModelTest 2: more models, new heuristics and high-performance computing. Nat. Methods 9, e772. https://doi.org/10.1038/nmeth.2109.

Debeljak, P., Baltar, F., 2023. Fungal diversity and community composition across ecosystems. J. Fungi 9, e510. https://doi.org/10.3390/jof9050510.

Duan, Y., Xie, N., Song, Z., Ward, C.S., Yung, C.-M., Hunt, D.E., Johnson, Z.I., Wang, G., 2018. A high-resolution time series reveals distinct seasonal patterns of planktonic fungi at a temperate coastal ocean site (Beaufort, North Carolina, USA). Appl. Environ. Microbiol. 84, e00967–18 https://doi.org/10.1128/AEM.00967-18.

Eggleton, P., Gaston, K.J., 1990. "Parasitoid" species and assemblages: convenient definitions or misleading compromises? Oikos 59, 417–421. https://doi.org/10.2307/3545155.

Enberg, S., Majaneva, M., Autio, R., Blomster, J., Rintala, J.-M., 2018. Phases of microalgal succession in sea ice and the water column in the Baltic Sea from autumn to spring. Mar. Ecol. Prog. Ser. 599, 19–34. https://doi.org/10.3354/meps12645.

Fernández-Valero, A.D., Reñé, A., Timoneda, N., Sampedro, N., Garcés, E., 2022. Dinoflagellate hosts determine the community structure of marine Chytridiomycota: demonstration of their prominent interactions. Environ. Microbiol. 24, 5951–5965. https://doi.org/10.1111/1462-2920.16182.

Fernández-Valero, A.D., Reñé, A., Timoneda, N., Pou-Solà, N., Gordi, J., Sampedro, N., Garcés, E., 2023. The succession of epiphytic microalgae conditions fungal community composition: how chytrids respond to blooms of dinoflagellates. ISME Commun. 3, e103. https://doi.org/10.1038/s43705-023-00304-x.

Garvetto, A., Badis, Y., Perrineau, M.-M., Rad-Menéndez, C., Bresnan, E., Gachon, C.M. M., 2019. Chytrid infecting the bloom-forming marine diatom *Skeletonema* sp.: morphology, phylogeny and distribution of a novel species within the Rhizophydiales. Fungal Biol. 123, 471–480. https://doi.org/10.1016/j.funbio.2019.04.004.

Gerphagnon, M., Latour, D., Colombet, J., Sime-Ngando, T., 2013. Fungal parasitism: life cycle, dynamics and impact on cyanobacterial blooms. PLOS ONE 8, e60894. https://doi.org/10.1371/journal.pone.0060894.

Grossart, H.-P., Wurzbacher, C., James, T.Y., Kagami, M., 2016. Discovery of dark matter fungi in aquatic ecosystems demands a reappraisal of the phylogeny and ecology of zoosporic fungi. Fungal Ecol. 19, 28–38. https://doi.org/10.1016/j.funeco.2015.06.004.

Guerrero, E., Abelló, P., Lombarte, A., Villanueva, R., Ramón, M., Sabatés, A., Santos, R., 2023. Marine Biological Reference Collections: CBMR-General (ICM-CSIC). Version 1.31. Instituto de Ciencias del Mar (CSIC). https://doi.org/10.15470/qlqqdx.

Guo, S.-Y., Jones, E.B.G., Chiang, M.W.L., Pang, K.-L., 2023. Salinity and temperature affect growth rate of *Alphamyces chaetifer* and *Gorgonomyces haynaldii* (Chytridiomycota) isolated from coastal habitats of Taiwan. Bot. Mar. 66, 345–352. https://doi.org/10.1515/bot-2023-0011.

Hassett, B.T., Vonnahme, T.R., Peng, X., Jones, E.B.G., Heuzé, C., 2019. Global diversity and geography of planktonic marine fungi. Bot. Mar. 63, 121–139. https://doi.org/10.1515/bot-2018-0113.

Jones, E.B.G., Ramakrishna, S., Vikineswary, S., Das, D., Bahkali, A.H., Guo, S.-Y., Pang, K.-L., 2022. How do fungi survive in the sea and respond to climate change? J. Fungi 8, e291. https://doi.org/10.3390/jof8030291.

Karpov, S.A., Reñé, A., Vishnyakov, A.E., Seto, K., Alacid, E., Paloheimo, A., Kagami, M., Kremp, A., Garcés, E., 2021. Parasitoid chytridiomycete *Ericiomyces syringoforeus* gen. et sp. nov. has unique cellular structures to infect the host. Mycol. Prog. 20, 95–109. https://doi.org/10.1007/s11557-020-01652-x.

Katoh, K., Standley, D.M., 2013. MAFFT multiple sequence alignment software version 7: improvements in performance and usability. Mol. Biol. Evol. 30, 772–780. https://doi.org/10.1093/molbev/mst010.

Lazarus, K.L., James, T.Y., 2015. Surveying the biodiversity of the Cryptomycota using a targeted PCR approach. Fungal Ecol. 14, 62–70. https://doi.org/10.1016/j.funeco.2014.11.004.

Lepelletier, F., Karpov, S.A., Alacid, E., Le Panse, S., Bigeard, E., Garcés, E., Jeanthon, C., Guillou, L., 2014. *Dinomyces arenysensis* gen. et sp. nov. (Rhizophydiales, Dinomycetaceae fam. nov.), a chytrid infecting marine dinoflagellates. Protist 165, 230–244. https://doi.org/10.1016/j.protis.2014.02.004.

López-García, P., Rodríguez-Valera, F., Pedrós-Alió, C., Moreira, D., 2001. Unexpected diversity of small eukaryotes in deep-sea Antarctic plankton. Nature 409, 603–607. https://doi.org/10.1038/35054537.

López-García, P., Philippe, H., Gail, F., Moreira, D., 2003. Autochthonous eukaryotic diversity in hydrothermal sediment and experimental microcolonizers at the Mid-Atlantic Ridge. Proc. Natl. Acad. Sci. U.S.A. 100, 697–702. https://doi.org/10.1073/pnas.0235779100.

Medina, E.M., Buchler, N.E., 2020. Chytrid fungi. Curr. Biol. 30, R516–R520. https://doi.org/10.1016/j.cub.2020.02.076.

Moreira, D., von der Heyden, S., Bass, D., López-García, P., Chao, E., Cavalier-Smith, T., 2007. Global eukaryote phylogeny: combined small- and large-subunit ribosomal

DNA trees support monophyly of Rhizaria, Retaria and Excavata. Mol. Phylogenet. Evol. 44, 255–266. https://doi.org/10.1016/j.ympev.2006.11.001.
Nunn, G.B., Theisen, B.F., Christensen, B., Arctander, P., 1996. Simplicity-correlated size growth of the nuclear 28S ribosomal RNA D3 expansion segment in the crustacean order isopoda. J. Mol. Evol. 42, 211–223. https://doi.org/10.1007/BF02198847.
Pernice, M.C., Forn, I., Gomes, A., Lara, E., Alonso-Sáez, L., Arrieta, J.M., del Carmen Garcia, F., Hernando-Morales, V., MacKenzie, R., Mestre, M., Sintes, E., Teira, E., Valencia, J., Varela, M.M., Vaqué, D., Duarte, C.M., Gasol, J.M., Massana, R., 2015. Global abundance of planktonic heterotrophic protists in the deep ocean. ISME J. 9, 782–792. https://doi.org/10.1038/ismej.2014.168.
Reñé, A., Alacid, E., Vishnyakov, A.E., Seto, K., Tcvetkova, V.S., Gordi, J., Kagami, M., Kremp, A., Garcés, E., Karpov, S.A., 2022. The new chytridiomycete *Paradinomyces triforaminorum* gen. et sp. nov. co-occurs with other parasitoids during a *Kryptoperidinium foliaceum* (Dinophyceae) bloom in the Baltic Sea. Harmful Algae 120, e102352. https://doi.org/10.1016/j.hal.2022.102352.
Reñé, A., Hoppenrath, M., 2019. *Psammodinium inclinatum* gen. nov. et comb. nov. (*Thecadinium inclinatum* Balech) is the closest relative to the toxic dinoflagellate genera *Gambierdiscus* and *Fukuyoa*. Harmful Algae 84, 161–171. https://doi.org/10.1016/J.HAL.2019.04.001.
Reñé, A., Timoneda, N., Sampedro, N., Alacid, E., Gallisai, R., Gordi, J., Fernández-Valero, A.D., Pernice, M.C., Flo, E., Garcés, E., 2021. Host preferences of coexisting Perkinsea parasitoids during coastal dinoflagellate blooms. Mol. Ecol. 30, 2417–2433. https://doi.org/10.1111/mec.15895.
Richards, T.A., Leonard, G., Mahé, F., del Campo, J., Romac, S., Jones, M.D.M., Maguire, F., Dunthorn, M., De Vargas, C., Massana, R., Chambouvet, A., 2015. Molecular diversity and distribution of marine fungi across 130 European environmental samples. Proc. R. Soc. B Biol. Sci. 282, e20152243. https://doi.org/10.1098/rspb.2015.2243.
Rojas-Jimenez, K., Rieck, A., Wurzbacher, C., Jürgens, K., Labrenz, M., Grossart, H.-P., 2019. A Salinity threshold separating fungal communities in the Baltic Sea. Front. Microbiol. 10, e680. https://doi.org/10.3389/fmicb.2019.00680.
Ronquist, F., Teslenko, M., van der Mark, P., Ayres, D.L., Darling, A., Höhna, S., Larget, B., Liu, L., Suchard, M.A., Huelsenbeck, J.P., 2012. MrBayes 3.2: Efficient Bayesian phylogenetic inference and model choice across a large model space. Syst. Biol. 61, 539–542. https://doi.org/10.1093/sysbio/sys029.
Scholin, C.A., Anderson, D.M., 1994. Identification of group -and strain-specific genetic markers for globally distributed *Alexandrium* (Dinophyceae). I. RFLP analysis of SSU rRNA Genes. J. Phycol. 30, 744–754. https://doi.org/10.1111/j.0022-3646.1994.00744.x.
Stamatakis, A., 2014. RAxML version 8: a tool for phylogenetic analysis and post-analysis of large phylogenies. Bioinformatics 30, 1312–1313. https://doi.org/10.1093/bioinformatics/btu033.
Tisthammer, K.H., Cobian, G.M., Amend, A.S., 2016. Global biogeography of marine fungi is shaped by the environment. Fungal Ecol. 19, 39–46. https://doi.org/10.1016/j.funeco.2015.09.003.
Trinci, A.P.J., Davies, D.R., Gull, K., Lawrence, M.I., Bonde Nielsen, B., Rickers, A., Theodorou, M.K., 1994. Anaerobic fungi in herbivorous animals. Mycol. Res. 98, 129–152. https://doi.org/10.1016/S0953-7562(09)80178-0.
Van den Wyngaert, S., Ganzert, L., Seto, K., Rojas-Jimenez, K., Agha, R., Berger, S.A., Woodhouse, J., Padisak, J., Wurzbacher, C., Kagami, M., Grossart, H.-P., 2022. Seasonality of parasitic and saprotrophic zoosporic fungi: linking sequence data to ecological traits. ISME J. 16, 2242–2254. https://doi.org/10.1038/s41396-022-01267-y.
Vaulot, D., Sim, C.W.H., Ong, D., Teo, B., Biwer, C., Jamy, M., Lopes dos Santos, A., 2022. metaPR2: a database of eukaryotic 18S rRNA metabarcodes with an emphasis on protists. Mol. Ecol. Resour. 22, 3188–3201. https://doi.org/10.1111/1755-0998.13674.
White, T.J., Bruns, T.D., Lee, S.B., Taylor, J.W., 1990. Amplification and direct sequencing of fungal ribosomal RNA genes for phylogenetics. In: Innis, M.A., Gelfand, D.H., Sninsky, J.J., White, T.J. (Eds.), PCR Protocols: A Guide to Methods and Applications. Academic Press, New York, N.Y., pp. 315–322. https://doi.org/10.1016/B978-0-12-372180-8.50042-1.
Xue, Y., Chen, H., Yang, J.R., Liu, M., Huang, B., Yang, J., 2018. Distinct patterns and processes of abundant and rare eukaryotic plankton communities following a reservoir cyanobacterial bloom. ISME J. 12, 2263–2277. https://doi.org/10.1038/s41396-018-0159-0.